P528 Notes #10: Collider Physics

David Morrissey
March 27, 2017

Most of what we know about the Standard Model (SM) at energies above a few hundred MeV comes from particle colliders. By colliding beams of known particles at high energies, we can produce new or unstable particles and study their properties [1, 2, 3]. This might sound terribly messy and violent, but in many cases it is the only probe we have, and the process has been refined to an exact science. In these notes we discuss some of the basic terminology and physics underlying modern particle colliders that you will need to understand research papers in the field [4, 5].

1 Modern High-Energy Paricle Colliders

Most recent high-energy particle colliders collide beams in the center-of-mass (CM) frame (*i.e.* the lab frame is the CM frame of the colliding particles). For a given beam energy, this maximizes the collision energy $\sqrt{s}$. Some of the most important modern high-energy colliders are:

- LEP I: e^+e^-, $\sqrt{s} \simeq m_Z$, ring; precision electroweak measurements (ALEPH, DELPHI, L3, OPAL).
- SLC/D: e^+e^-, $\sqrt{s} \simeq m_Z$, linear; precision electroweak measurements.
- LEP II: e^+e^-, $\sqrt{s} = m_Z - 208$ GeV, ring; electroweak measurements, Higgs searches, New Physics (ALEPH, DELPHI, L3, OPAL).
- Tevatron: $p\bar{p}$, $\sqrt{s} = 1.8$–1.96 TeV, ring; top quarks, electroweak measurements, Higgs, New Physics (CDF, $D\emptyset$).
- LHC: pp, $\sqrt{s} = 7$–14 TeV, ring; Higgs, New Physics (ATLAS, CMS, LHCb, ALICE).
- ILC (proposed): e^+e^-, $\sqrt{s} = 500 - 1000$ GeV, linear; Higgs, New Physics.
- CLIC (proposed): e^+e^-, $\sqrt{s} = 1000 - -3000$ GeV, linear: Higgs, New Physics.

Here, we have listed the beam types, the collision energy, the collider geometry (ring or linear), the primary physics objectives, and a list of the main detector experiments at the collider (when there is more than one).

The two main collider geometries are ring and linear. In the ring geometry, the two beams circulate in opposite directions around a roughly circular beam pipe. At a few locations along the ring the beams are brought together to collide. For obvious reasons, fancy detectors are placed around these collision points. We show the setup of the LHC in Fig. 1. The diameter of the LHC (and LEP) ring is about 27 km while the Tevatron ring is about 6 km

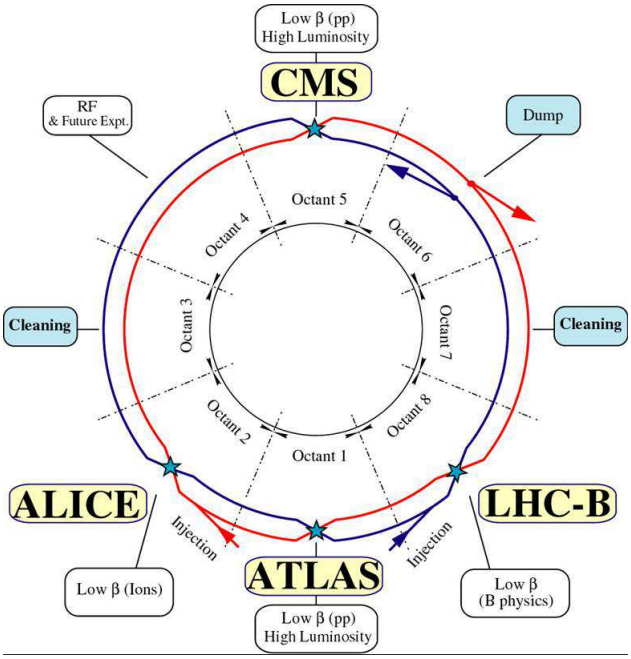

Figure 1: Collider rings and detectors at the LHC.

in diameter. Ring colliders allow for multiple collision points and are relatively compact. Their main disadvantage is that accelerating light particles such as electrons around the ring can lead to severe energy losses to radiation. For this reason, very high energy electron-positron colliders are typically linear, consisting of two straight accelerating segments. These segments are about 3 km long at SLC/D and are expected to be about 20 km long at the ILC. This is less compact than a ring geometry, and only allows for a single collision point.

The LEP, SLC/D, and ILC colliders use e^+e^- beams. Since electrons and positrons are fundamental particles, this leads to relatively simple collisions with the full beam energy. They can also be polarized (in their spins), allowing one to study LH and RH fermion couplings in isolation. The downside is that it is more difficult (engineering-wise) to make a very high-energy electron beam. On the other hand, the Tevatron ($p\bar{p}$) and the LHC (pp) are hadron colliders. This allows for larger collision energies, but at a cost. Hadron collisions are very complicated because they involve composite objects. This implies that we do not know the longitudinal boost of the collision (unless we measure it directly), and that the actual collision energy is less than the full beam energy. Recall that for colliding partons with momentum fractions x_1 and x_2, the parton collision energy is

$$\sqrt{\hat{s}} = \sqrt{x_1 x_2}\sqrt{s} \tag{1}$$

and the net longitudinal (along the beam direction) component of the momentum in the lab frame is

$$(x_1 - x_2)\sqrt{s}/2. \tag{2}$$

This net boost leads to complications when there are unseen particles in the event.

The two main parameters of the colliding beams are the collision energy and the luminosity. The highest consistent collision energy achieved so far is about $\sqrt{s} = 13$ TeV at the LHC, which is considerably higher than the previous record set by the Tevatron of $\sqrt{s} = 1.96$ TeV. The luminosity of the beam is the net colliding particle flux, and is typically expressed in units of $\mathrm{cm}^{-2}\mathrm{s}^{-1}$. In practice, most collider beams consist of distinct bunches of particles. For two beams with bunches containing N_1 and N_2 particles per bunch respectively, each separated by a timing gap of $\tau = 1/f$ and with cross-sectional area A, the net luminosity is basically (assuming uniform bunch densities)

$$\mathcal{L} = \frac{N_1 N_2}{\tau A} \ . \tag{3}$$

The total event rate for a given process is then

$$\frac{dN}{dt} = \sigma \, \mathcal{L} \ , \tag{4}$$

where σ is the corresponding scattering cross section. The total amount of data recorded in collider experiments is usually expressed in terms of the integrated luminosity

$$\mathcal{L}_{int} = \int dt \, \mathcal{L} \ . \tag{5}$$

Evidently $\sigma \, \mathcal{L}_{int}$ is the total number of events. It is therefore standard to express the integrated luminosity in units of inverse cross-section,

$$1 \, \mathrm{fb}^{-1} = 10^3 \, \mathrm{pb}^{-1} = 10^6 \, \mathrm{nb}^{-1} = 10^{39} \, \mathrm{cm}^{-2} \ . \tag{6}$$

At the LHC, consistent luminosities over $10^{34} \, \mathrm{cm}^{-2}\mathrm{s}^{-1}$ have been achieved, corresponding to an integrated luminosity of roughly $100 \, \mathrm{fb}^{-1}$ per year [6].

2 Collider Detectors

Sensitive particle detectors are placed around the locations where the beams in particle collider meet. Their role is to measure the products of the collisions. Doing so, the underlying hard scattering event can often be reconstructed to learn about the underlying fundamental particles and forces.

A cartoon of a typical modern particle detector is given in Fig. 2. It is roughly cyclindrical around the beam (z) axis, and we show both a side and a cross-sectional view. From the inside closest to the beam and moving out, the layers are VX = vertexing, TR = tracking, ECAL = electromagnetic calorimeter, HCAL = hadronic calorimeter, MC = muon chamber. There is also typically a magnetic field parallel to the z axis within the tracking chamber. The roles of the various layers are:

- The VX and TR layers measure the tracks of charged particles passing through them. Since there is a magnetic field within these layers, the trajectories of charged particles will be curved, with a radius of curvature proportional to

$$R \propto QB/p \ . \tag{7}$$

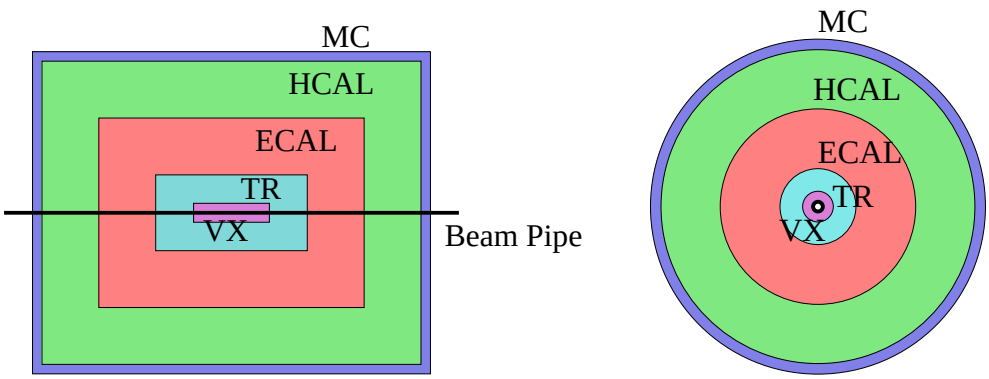

Figure 2: Side (left) and cross-sectional (right) views of a typicle particle detector. The beam lies along the z axis, VX = vertexing, TR = tracking, ECAL = electromagnetic calorimeter, HCAL = hadronic calorimeter, MC = muon chamber.

This allows for a measurment of Q/p for the particles passing through.

- The ECAL captures and measures the energies of electrons and photons.
- The HCAL captures and meaures the energies of hadronic particles.
- The MC measures the passage of muons. These particles are very difficult to stop and punch through all the layers. The MC finds the tracks of through-going muons, allowing for a measurement of the muon momentum by way of the curvature of its track (matched to the VX and TR tracks).

With such a detector structure, there is a corresponding basic set of reconstructed *detector objects* that correspond to (sets) of SM particles. The standard objects are:

- QCD jets: charged tracks in the VX and TR layers (usually), significant energy deposition in both the ECAL and HCAL.
- $e^{\pm}$: charged tracks in the VX and TR layers, energy deposition primarily in the ECAL.
- γ: no charged tracks, energy deposition primarily in the ECAL.
- $\mu^{\pm}$: charged tracks in the VX and TR layers, small energy in the ECAL and HCAL, detector hits in the MC.

Vertexing also allows one to identify jets containing b (and sometimes c) quarks.

The radius of a typical detector is on the order of few meters. It is instructive to compare this to the *decay length* travelled by various SM particles before they decay:

$$d = \gamma\, v\, \tau \simeq \gamma\, v\, (300\,\mu\text{m}) \left(\frac{\tau}{10^{-12}\,\text{s}}\right) \ , \tag{8}$$

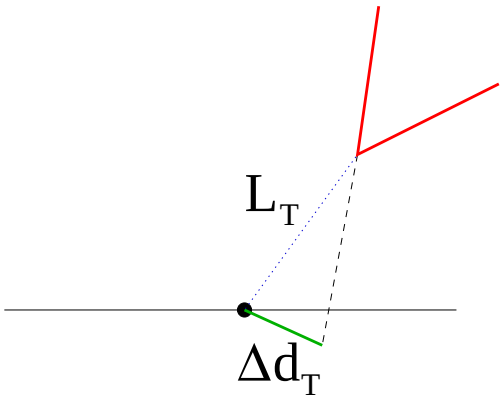

Figure 3: Geometry of a displaced vertex in the plane transverse to the beam.

where $\gamma = E/m = 1/\sqrt{1-v^2}$ and τ is the lifetime in the particle rest frame. By comparison, we have

$$\tau_{t,W,Z} \sim 10^{-25}\,\mathrm{s}\,, \tag{9}$$

so that W, Z, and t parcicles effectively decay instantaneously. The time scale for showering and hadronization of QCD jets is roughly

$$\tau_{QCD} \sim \Lambda_{QCD}^{-1} \sim 10^{-24}\,\mathrm{s}\,, \tag{10}$$

so this complicated process is also essentially instantaneous. For the unstable leptons,

$$\tau_{\mu} \sim 10^{-6}\,\mathrm{s}\,, \qquad \tau_{\tau} \sim 10^{-13}\,\mathrm{s}\,, \tag{11}$$

and thus the μ is long-lived with respect to the detector while the τ decays quickly. Among the mesons, it is found that

$$\tau_{\pi^{\pm}} \sim 10^{-8}\,\mathrm{s}, \quad \tau_{\pi^0} \sim 10^{-16}\,\mathrm{s}, \quad \tau_{K^{\pm,0_s}} \sim 10^{-8}\,\mathrm{s}, \quad \tau_B \sim 10^{-12}\,\mathrm{s}, \quad \tau_D \sim 10^{-12}\,\mathrm{s}\,. \tag{12}$$

The lifetimes of the B and D mesons lie in a range that can be detected by the VX systems of the detectors at the Tevatron and the LHC. This permits b- and c-tagging of hadronic jets, where the underlying jet is identified as coming from a b or c quark. Starting from a b quark, for example, it will hadronize nearly immediately into a B meson together with some other hadrons consisting of gluons and light quarks. The B meson will decay after travelling a microscopic distance L_T in the plane transverse to the beam. The decay products of the B meson will leave their own tracks if they are charged. The essential feature is that these tracks need not point back to the beam interaction point, but rather to a location that is somewhat displaced. We illustrate this in Fig. 3. Such *displaced vertices* are characteristic of jets initiated by a b or c quark. The amount of displacement in the transverse plane is on the order of

$$\Delta d_T \simeq L_T \theta, \tag{13}$$

where $\theta \sim \gamma^{-1}$ is the opening angle of the B meson decay products. The vertexing systems at the LHC can achieve a resolution on the order of $20\,\mu$m, allowing for a relatively efficient identification of b and c jets. A somewhat related technique can be used to identify τ leptons.

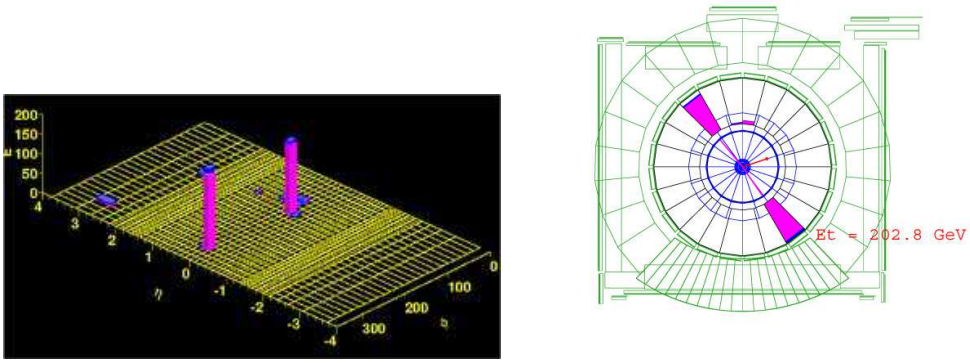

Figure 4: An e^+e^- event at CDF shown in terms of a lego plot of the ECAL cell energies (left) and also in terms of which cells in the detector received hits (right).

3 Kinematics

The calorimeters and the muon chambers in a particle detector are segmented into *cells*. This allows for the reconstruction of the 4-momentum of any detector object. Relative to the detector geometry, a useful set of coordinates for the 4-momenta are (p_T, η, ϕ). Here, p_T is the magnitude of the momentum of the particle (or jet) projected onto the transverse plane orthogonal the beam direction (*i.e.* the x-y plane),

$$p_T = \|\vec{p}\| \sin\theta \ . \tag{14}$$

The quantity η is called the pseudo-rapidity and is related to the polar angle θ from the beam according to

$$\eta = \frac{1}{2} \ln\left(\frac{1+c_\theta}{1-c_\theta}\right) = \ln\left[\cot\left(\frac{\theta}{2}\right)\right] \ . \tag{15}$$

Note that the beams coincide with $\eta \to \pm\infty$ and $\eta = 0$ defines the transverse plane. Finally, ϕ is the azimuthal angle in the transverse plane. These variables range over $\phi \in [0, 2\pi]$, $\eta \in (-\infty, \infty)$, and $p_T \in (0, \infty)$.

The cell structure of a calorimeter typically coincides with a segmentation in terms of $\Delta\eta$ and $\Delta\phi$. Typically, objects with $|\eta| \lesssim 2.5$ are called *central* and objects with $|\eta| \gtrsim 2.5$ are said to be *forward*. The detectors are most finely-segmented in the central region, but forward coverage also plays a very important role in many searches. Events at colliders are often portrayed in terms of "lego plots" which explicitly display the cell structure of the detector. We show such a plot in Fig. 4.

For jets and related objects it is frequently useful to use cones defined in terms of the η and ϕ variables. The cone opening angle is usually written as

$$\Delta R = \sqrt{(\Delta\eta)^2 + (\Delta\phi)^2} \ . \tag{16}$$

Opening angles of $\Delta R \simeq 0.4$ are fairly typical for central jets.

Sometimes the kinematics of a detector object are written in terms of the *rapidity* y rather than the pseudo-rapidity η. The rapidity is defined to be

$$y = \frac{1}{2} \ln \left(\frac{E + p_z}{E - p_z} \right) \ . \tag{17}$$

It reduces to the pseudo-rapidity in the limit that the particle is massless. We can also express the 4-momentum of any detector object in terms of the rapidity according to

$$p^\mu = (E_T \cosh y, p_T \cos\phi, p_T \sin\phi, E_T \sinh y) \ , \tag{18}$$

where $E_T = \sqrt{p_T^2 + m^2}$.

4 Particle Identification at Hadron Colliders

We turn now to discuss some techniques for identifying particles produced at hadron colliders.

4.1 Z Bosons and Invariant Momentum

We discussed previously the production of Z gauge bosons at e^+e^- colliders [7]. Recall that by scanning over over the collision energy, it is possible to map out the Z-pole resonance by plotting the cross-section for $e^+e^- \to f\bar{f}$ as a function of $\sqrt{s}$. This resonance comes from the Z propagator factor in the matrix element, which becomes very large for $\sqrt{s} \simeq m_Z$.

Things are bit different at hadronic (pp or $p\bar{p}$) colliders. Most importantly, the parton-level collision energy varies from event to event,

$$\hat{s} = x_1 x_2 \, s. \tag{19}$$

On the one hand, this makes our life more difficult because we don't have control over the parton-level collision energy within any particular event. But on the other, it implies that by looking at many events we automatically scan over the parton collision energy. This gives us a straightforward way to identify the Z^0 boson in hadron collision events such as $q\bar{q} \to \mu^+\mu^-$.

Focussing on the process $p\bar{p} \to \mu^+\mu^-$, the objects measured by the detector are the 4-momenta p_{μ^+} and p_{μ^-} of the outgoing muons. This process gets contributions (at the leading order) from diagrams with a γ or a Z^0 in the s channel connecting to a $q\bar{q}$ pair in the initial state. By momentum conservation, we know that the momentum of the intermediate vector boson is $q = (p_{\mu^+} + p_{\mu^-})$. This motivates us to define the (dimuon) *invariant mass*

$$m^2_{\mu^+\mu^-} = (p_{\mu^+} + p_{\mu^-})^2 = \hat{s}. \tag{20}$$

By making a histogram of the number of events observed per unit invariant mass, we should see a distinct peak around $m_{\mu^+\mu^-} = m_Z$. Such a peak is seen within the data, as shown in Fig. 5 for the CDF experiment at the Tevatron.

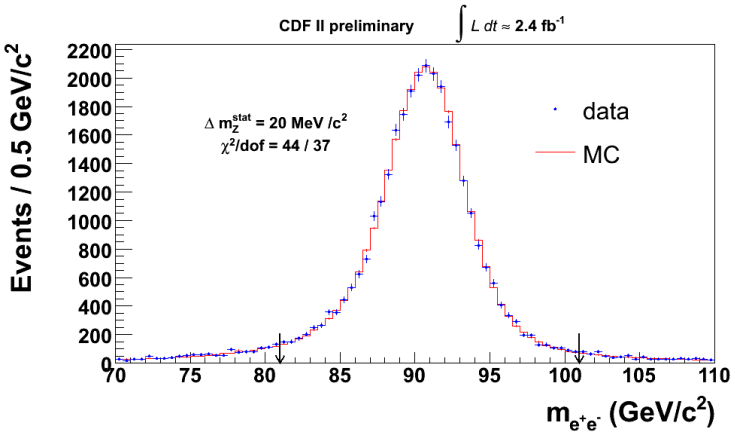

Figure 5: Distribution of $\mu^+\mu^-$ events seen my the CDF experiment at the Tevatron with respect to the dimuon invariant mass.

More generally, we can form an invariant mass from the square of the sum of any set of 4-vectors. This is useful, for example, in searching for the Higgs boson. For Higgs masses above about $2m_Z$, one of the most promising search modes is $gg \to h \to ZZ \to 4\ell$. By forming pairs of dilepton invariant masses, we can reconstruct the intermediate Z^0 particles (which almost always on-shell for $m_h > 2m_Z$). Summing up the 4-vectors of all four leptons and taking the invariant square, we should see a distinct peak at the location of the Higgs mass.

4.2 W Bosons and Transverse Mass

When looking for W bosons at hadron colliders, it would be nice to use the same invariant mass trick as for the Z. Unfortunately, only the leptonic decay mode $W^- \to \ell\bar{\nu}_\ell$ can be extracted from the large QCD background ($W^- \to q\bar{q}'$ is swamped). For such decays, only the lepton is observed directly since the neutrino simply passes through the detector without leaving a trace. This makes it impossible to form the invariant mass variable $m^2_{\nu\ell} = (p_\nu + p_\ell)^2$ that would produce a peak at the W mass. Despite this complication, it is still possible to obtain a kinematic distribution that is characteristic of the W and that allows for extraction of its mass.

Even though the neutrino doesn't leave a signal in the detector, its presence can be deduced indirectly from momentum conservation. With only a visible lepton, the net observed momentum in the transverse plane of the final state is non-zero, even though the transverse momentum of the initial state (consisting of quarks and gluons in the protons) has a transverse momentum less than about Λ_{QCD}. This imbalance in the observed transverse momentum $\vec{p}_T$ is called *missing momentum* and it indicates the presence of an unobserved particle (to the extent that we trust momentum conservation, which we do). In general, the

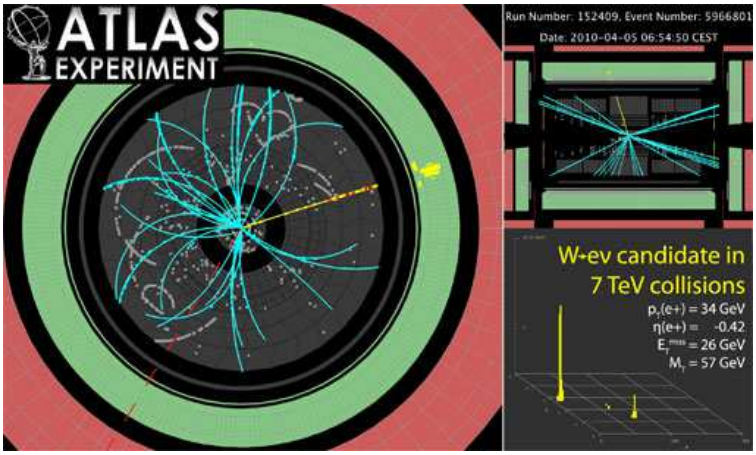

Figure 6: Event display and lego plot of a candidate $W \to e\nu$ event observed by ATLAS.

missing momentum $\not{p}_T$ in an event is given by

$$\not{p}_T = -\sum_{vis} \vec{p}_T, \tag{21}$$

where the sum runs over all visible objects seen by the detector. The magnitude of $\not{p}_T$ is sometimes called the missing transverse energy $\not{E}_T$. Note that since we don't know the net longitudinal boost of the parton system in hadron collisions, we are not able to use the same trick for the longitudinal momentum components.

For leptonic W decays, we have

$$\not{p}_T \simeq -\vec{p}_{T\,\ell}. \tag{22}$$

In terms of $\not{E}_T$ and $\vec{p}_{T\,\ell}$ we can form the *transverse mass*

$$\begin{aligned} m_T^2 &= (E_{T\,\ell} + \not{E}_T)^2 - (\vec{p}_{T\,\ell} + \not{p}_T)^2 \\ &= 2p_{T\,\ell}\cdot p_{T\,\nu} \\ &= E_{T\,\ell}E_{T\,\nu}(1-\cos\theta_{\nu\ell}), \end{aligned} \tag{23}$$

where $E_{T\,\ell} = \sqrt{p_{T\,\ell}^2 + m_\ell^2}$ and $p_{T\,i} = (E_{T\,i}, \vec{p}_{T\,i})$. It is not hard to show that $m_T^2 \le m_W^2$ when the W is on-shell. By plotting hadron collider event rates as a function of m_T, we find a distinctive upper edge in the distribution. We show such a distribtion obtained by the CDF experiment at the Tevatron in Fig. 7. It is possible to extract the mass of the W from the shape of this distribution.

4.3 Top Quarks

Top quarks were first discovered about fifteen years ago at the Tevatron. They are much heavier than all the other known quarks ($m_t = 172.0 \pm 2.2$ GeV) and behave much differently

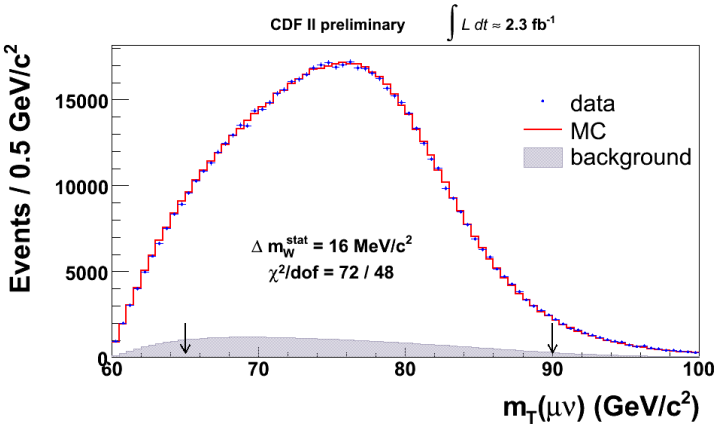

Figure 7: Distribution of $W \to \mu\nu$ events with the transverse mass m_T seen by CDF.

from the others when they are produced in particle colliders. Most significantly, their decay rate is on the order of $\tau_t \sim 10^{-25}\, s$, which is significantly faster than the time needed to hadronize, $\tau_{QCD} \sim 10^{-24}\, s$. As a result, we can compute their decays within perturbative QCD and trust the answer. Nearly every t quark decays to $t \to W^+ b$.

The main production mechanism for top quarks at both the Tevatron and the LHC is in the form of $t\bar{t}$ pairs [8, 9]. (A $t\bar{b}$ combination with a single top can be produced by a W^+ in the s-channel but with a smaller rate.) This leads to two b-jets, and a W^+W^- pair in every event. The $W^\pm$ can decay leptonically via $W^- \to \ell\bar{\nu}_{ell}$ or hadronically through $W^- \to q\bar{q}'$. Most studies of top quarks at hadron colliders therefore focus on three channels: i) hadronic; ii) lepton + jets; iii) dileptons.

The hadronic channel is characterized by six (or more) jets of which at least two have b-tags. The non-b jets can be combined in pairs to form invariant mass combinations. When the "right" pair is chosen, corresponding to both jets coming from the same W decay, it should reconstruct the W mass, $m^2_{j_1 j_2} = (p_{j_1} + p_{j_2})^2 \simeq m^2_W$. Combining all these correct pairs of jets with the right b jet will then reconstruct the top mass, $m^2_{j_1 j_2 b} = (p_{j_1} + p_{j_2} + p_b)^2 \simeq m^2_t$. Using these kinematic requirements together with b-tagging, it is possible to extract the signal from a large QCD background.

The lepton + jets channel contains one lepton, four jets of which at least two have b-tags, and missing energy from the neutrino. The top mass can be reconstructed from the hadronic W decay as above. Backgrounds come primarily from QCD and W+jets.

In the dilepton channel there are two leptons with opposite signs, missing energy, and two b-tagged jets. It is not possible to reconstruct the kinematics of these events without making additional assumptions. The main sources of backgrounds are W+jets and Z+jets.

References

[1] T. Han, "Collider phenomenology: Basic knowledge and techniques," [hep-ph/0508097].

[2] T. Plehn, "Lectures on LHC Physics," [arXiv:0910.4182 [hep-ph]].

[3] M. Perelstein, "Introduction to Collider Physics," [arXiv:1002.0274 [hep-ph]].

[4] G. Aad *et al.* [The ATLAS Collaboration], "Expected Performance of the ATLAS Experiment - Detector, Trigger and Physics," [arXiv:0901.0512 [hep-ex]].

[5] CMS Collaboration, "Physics Technical Design Report", http://cmsdoc.cern.ch/cms/cpt/tdr/

[6] ATLAS Collaboration, "Luminosity Public Results," https://twiki.cern.ch/twiki/bin/view/AtlasPublic/LuminosityPublicResultsRun2

[7] Lecture Notes #7

[8] F. Deliot, D. A. Glenzinski, "Top Quark Physics at the Tevatron," [arXiv:1010.1202 [hep-ex]].

[9] G. Aad *et al.* [Atlas Collaboration], "Measurement of the top quark-pair production cross section with ATLAS in pp collisions at $\sqrt{s} = 7$ TeV," [arXiv:1012.1792 [hep-ex]].